

Experimental realization of nonadiabatic geometric gates with a superconducting Xmon qubit

P. Z. Zhao,¹ Zhangjingzi Dong,² Zhenxing Zhang,² Guoping Guo,^{3,4} D. M. Tong,^{1,*} and Yi Yin^{2,†}

¹*Department of Physics, Shandong University, Jinan 250100, China*

²*Department of Physics, Zhejiang University, Hangzhou 310027, China*

³*Key Laboratory of Quantum Information, University of Science and Technology of China, Hefei, 230026, China*

⁴*Origin Quantum Computing, Hefei, 230026, China*

(Dated: September 24, 2019)

Geometric phases are only dependent on evolution paths but independent of evolution details so that they own some intrinsic noise-resilience features. Based on different geometric phases, various quantum gates have been proposed, such as nonadiabatic geometric gates based on nonadiabatic Abelian geometric phases and nonadiabatic holonomic gates based on nonadiabatic non-Abelian geometric phases. Up to now, nonadiabatic holonomic one-qubit gates have been experimentally demonstrated with the superconducting transmon, where three lowest levels with cascaded configuration are all applied in the operation. However, the second excited states of transmons have relatively short coherence time, which results in a lessened fidelity of quantum gates. Here, we experimentally realize Abelian-geometric-phase-based nonadiabatic geometric one-qubit gates with a superconducting Xmon qubit. The realization is performed on two lowest levels of an Xmon qubit and thus avoids the influence from the short coherence time of the second excited state. The experimental result indicates that the average fidelities of single-qubit gates can be up to 99.6% and 99.7% characterized by quantum process tomography and randomized benchmarking, respectively.

I. INTRODUCTION

The implementation of circuit-based quantum computation requires to realize a universal set of accurately controllable quantum gates, including arbitrary one-qubit gates and a non-trivial two-qubit gate [1]. However, the errors resulting from the imperfect control of quantum systems inevitably affect quantum gates. This motivates researchers to utilize the features of geometric phases to suppress control errors. Geometric phases are only dependent on evolution paths but independent of evolution details so that the quantum gates based on geometric phases own some intrinsic noise-resilience features [2–7]. The early schemes of geometric-phase-based quantum computation [8–10] is realized by using adiabatic geometric phases [11, 12]. However, the long run time required by the adiabatic evolution makes quantum gates vulnerable to the environment-induced decoherence. To overcome this problem, nonadiabatic geometric quantum computation [13, 14] based on nonadiabatic Abelian geometric phases [15] was proposed and further nonadiabatic holonomic quantum computation [16, 17] based on nonadiabatic non-Abelian geometric phases [18] was put forward.

Nonadiabatic Abelian geometric phases are generated by the cyclic evolution of quantum states with removal of dynamical phases and the computational space itself is enough for the realization of nonadiabatic geometric gates. Correspondingly, nonadiabatic non-Abelian geometric phases are generated by the cyclic evolution and parallel transport of a state subspace in the Hilbert space so that the realization of nonadiabatic holonomic gates needs the computation space in addition to auxiliary states. Since nonadiabatic geometric quantum computation as well as nonadiabatic holonomic quantum computation not only has some intrinsic noise-resilience

features but also allow high-speed implementation, they have received increasing attention [19–49]. Up to now, nonadiabatic geometric gates have been experimentally demonstrated with trapped ions [35] and nuclear magnetic resonance [36], and nonadiabatic holonomic gates have been experimentally demonstrated with nuclear magnetic resonance [37, 38], superconducting [39–43], and nitrogen-vacancy centers in diamond [44–49]. Besides, adiabatic geometric gates have been sped up [50, 51] by using transitionless quantum driving algorithm [52] and the corresponding experiments have demonstrated this result [53–55].

The superconducting circuit provides an appealing experimental platform for the implementation of quantum computation since the integrated circuit can be easily scaled up to multi-qubit systems and each qubit can be controlled by individual lines. As a charge-insensitive superconducting qubit [56], the transmon has been used for the experimental realization of nonadiabatic holonomic one-qubit gates [39–42], where three lowest levels with cascaded configuration are used as a quantum system. However, the second excited states of transmons have relatively short coherence time, which results in a lessened fidelity of quantum gates. This motivates us to use nonadiabatic Abelian geometric phase to experimentally realize nonadiabatic geometric gates since the realization only needs a two-level computational space and does not require the extra auxiliary level.

In this paper, we experimentally realize nonadiabatic geometric one-qubit gates with a cross-shaped transmon qubit, named Xmon qubit [57–59]. The superconducting Xmon qubit is a high-quality qubit because it not only possesses relatively long coherence time but also balances coherence, connectivity, and fast control with specific designing. Our realization is performed on two lowest levels of the Xmon qubit and thus avoids the influence from the short coherence time of the second excited state. By using the slice-shaped evolution path of two orthogonal quantum states [32], we can realize an arbitrary nonadiabatic geometric one-qubit gate by a single

* tdm@sdu.edu.cn

† yyin@zju.edu.cn

loop. In our experiment, we demonstrate some specific nonadiabatic geometric gates. The average fidelities of the gates can be up to 99.6% and 99.7% characterized by quantum process tomography and randomized benchmarking, respectively.

II. THE PROTOCOL

Our protocol is based on nonadiabatic Abelian geometric phases. We first explain how the nonadiabatic Abelian geometric phases arise [15]. Consider a quantum state $|\psi(t)\rangle$ exposed to the Hamiltonian $H(t)$ satisfying Schrödinger equation $i\dot{|\psi(t)\rangle} = H(t)|\psi(t)\rangle$. If the state $|\psi(t)\rangle$ undergoes cyclic evolution, the initial state $|\psi(0)\rangle$ acquires a phase

$$\gamma(\tau) = i \int_0^\tau \langle \dot{\psi}(t) | \dot{\psi}(t) \rangle dt - \int_0^\tau \langle \psi(t) | H(t) | \psi(t) \rangle dt, \quad (1)$$

where $|\dot{\psi}(t)\rangle$ is an auxiliary state satisfying $|\psi(0)\rangle = |\dot{\psi}(0)\rangle = |\dot{\psi}(\tau)\rangle$. Here, the first part of the phase $\gamma(t)$ is known as geometric phases and the second part is known as dynamical phases. Further, if the dynamical phase is equal to zero, then $\gamma(\tau)$ yields a pure geometric phase.

We then demonstrate how to realize an arbitrary single-qubit nonadiabatic geometric gate with a superconducting Xmon qubit. Consider a two-level Xmon qubit consisting of ground state $|0\rangle$ and the first excited state $|1\rangle$. The transition $|0\rangle \leftrightarrow |1\rangle$ is facilitated by a resonant microwave pulse with time-dependent Rabi frequency $\Omega(t)$. In the rotating frame, the Hamiltonian under the rotating wave approximation reads

$$H(t) = \Omega(t)|0\rangle\langle 1| + \text{H.c.}, \quad (2)$$

where H.c. represents the Hermitian conjugate terms.

To realize the nonadiabatic geometric gates, we divide the whole evolution period τ into three intervals $0 \sim \tau_1$, $\tau_1 \sim \tau_2$ and $\tau_2 \sim \tau$, each of which is with a different microwave phase parameter. The Hamiltonian in the first interval $0 \sim \tau_1$ and the third interval $\tau_2 \sim \tau$ is taken as

$$H_1(t) = \Omega_R(t)e^{-i(\varphi - \frac{\gamma}{2})}|0\rangle\langle 1| + \text{H.c.}, \quad (3)$$

and the Hamiltonian in the second interval $\tau_1 \sim \tau_2$ is taken as

$$H_2(t) = \Omega_R(t)e^{-i(\varphi - \frac{\gamma}{2} + \frac{\pi}{2})}|0\rangle\langle 1| + \text{H.c.}, \quad (4)$$

where $\Omega_R(t)$ is the time-dependent microwave amplitude parameter, and φ and γ are the time-independent microwave phase parameters. Meanwhile, the evolution time τ_1 , τ_2 and τ are taken to satisfy

$$\begin{aligned} \int_0^{\tau_1} \Omega_R(t) dt &= \frac{\theta}{2}, & \int_{\tau_1}^{\tau_2} \Omega_R(t) dt &= \frac{\pi}{2}, \\ \int_{\tau_2}^{\tau} \Omega_R(t) dt &= \frac{\pi}{2} - \frac{\theta}{2}. \end{aligned} \quad (5)$$

With this design, two orthogonal states $|\psi_+\rangle = \cos(\theta/2)|0\rangle + \sin(\theta/2)\exp(i\varphi)|1\rangle$ and $|\psi_-\rangle = \sin(\theta/2)\exp(-i\varphi)|0\rangle - \cos(\theta/2)|1\rangle$ undergo cyclic evolution,

$$\begin{aligned} |\psi_+\rangle &\rightarrow U(\tau)|\psi_+\rangle = e^{-i\frac{\gamma}{2}}|\psi_+\rangle, \\ |\psi_-\rangle &\rightarrow U(\tau)|\psi_-\rangle = e^{i\frac{\gamma}{2}}|\psi_-\rangle, \end{aligned} \quad (6)$$

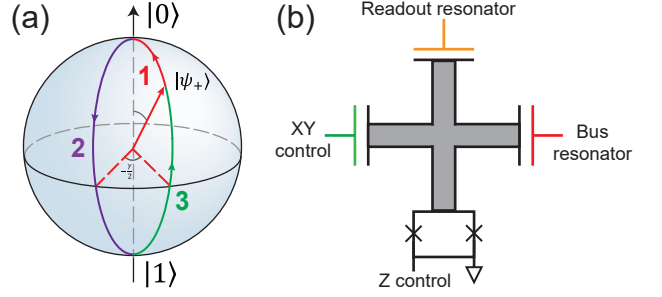


FIG. 1. (Color online) The schematic setup for realization of nonadiabatic geometric gates. (a) The evolution path of state $|\psi_+\rangle$ with Bloch sphere representation. The state $|\psi_+\rangle$ is driven by the designed microwave pulses along an orange slice-shaped path in the computational space and acquires a geometric phase $-\gamma/2$. (b) The cross-shaped architecture of superconducting Xmon.

and they respectively acquire phases $-\gamma/2$ and $\gamma/2$, where $U(\tau)$ is the final evolution operator reading

$$U(\tau) = e^{-i \int_{\tau_2}^{\tau} H_1(t) dt} e^{-i \int_{\tau_1}^{\tau_2} H_2(t) dt} e^{-i \int_0^{\tau_1} H_1(t) dt}. \quad (7)$$

We can verify that the dynamical phases γ_{d_\pm} acquired by $|\psi_\pm\rangle$ are equal to zero, i.e., $\gamma_{d_\pm} = -\int_0^{\tau_1} \langle \psi_\pm(t) | H_1(t) | \psi_\pm(t) \rangle dt - \int_{\tau_1}^{\tau_2} \langle \psi_\pm(t) | H_2(t) | \psi_\pm(t) \rangle dt - \int_{\tau_2}^{\tau} \langle \psi_\pm(t) | H_1(t) | \psi_\pm(t) \rangle dt = 0$, where $|\psi_\pm(t)\rangle = U(t)|\psi_\pm\rangle$ with $U(t)$ being the evolution operator. Therefore, $-\gamma/2$ and $\gamma/2$ are pure geometric phases. By using the visualization Bloch sphere representation for the evolution of state $|\psi_+\rangle$, γ is indeed proportional to the solid angle enclosed by the orange-slice-shaped loop, shown in Fig. 1(a). From Eq. (6), we can readily find that the evolution operator $U(\tau)$ can be equivalently expressed as

$$U(\tau) = e^{-\frac{\gamma}{2}}|\psi_+\rangle\langle\psi_+| + e^{\frac{\gamma}{2}}|\psi_-\rangle\langle\psi_-| = e^{-i\gamma\mathbf{n}\cdot\boldsymbol{\sigma}/2}, \quad (8)$$

where $\mathbf{n} = (\sin\theta\cos\varphi, \sin\theta\sin\varphi, \cos\theta)$ and $\boldsymbol{\sigma} = (\sigma_x, \sigma_y, \sigma_z)$ being the Pauli operators acting on $|0\rangle$ and $|1\rangle$. As discussed above, $-\gamma/2$ and $\gamma/2$ are pure geometric phases, thus $U(\tau)$ is a nonadiabatic geometric gate. By using this geometric gate $U(\tau)$, we can realize an arbitrary one-qubit gate, where the rotation axis is determined by $\{|\psi_+\rangle, |\psi_-\rangle\}$ and the rotation angle is determined by γ .

III. THE EXPERIMENT

In our experiment, the superconducting Xmon is an aluminum-based circuit, which is operated at temperature about 10mK in a cryogen-free dilution refrigerator. The Xmon sample is fabricated on a silicon substrate using a standard nano-fabrication method. The Xmon device is designed with cross-shaped architecture, shown in Fig. 1(b). The four arms of Xmon device connect to four separate elements with different functions. The key element of the qubit is the pair of Josephson junctions at the bottom, which form a rectangular ring-shaped superconducting quantum interference device. The qubit frequency is tuned by the Z control line. The readout resonator on the top is for the measurement of qubit states.

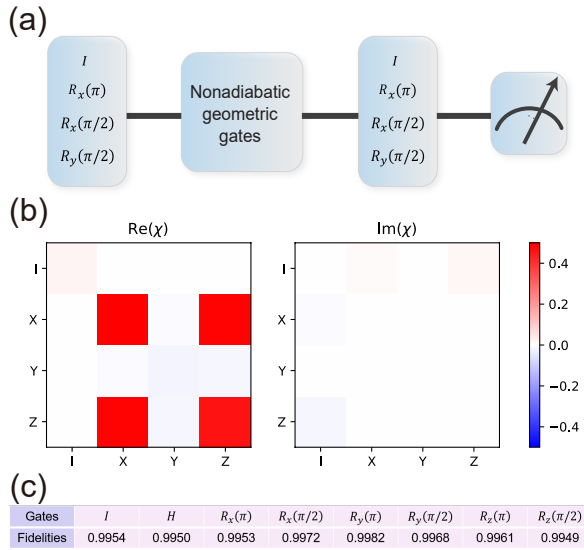


FIG. 2. (Color online) Quantum process tomography for nonadiabatic geometric gates. (a) The schematic diagram for quantum process tomography. (b) The matrix elements generated by Hadamard gate H with real part on the left and imaginary part on the right. (c) The process fidelities of nonadiabatic geometric gates.

The XY control on the left is used for the manipulation of qubit states by inputting microwave pulses. Through the right arm, the qubit can be coupled to a quantum bus resonator or another qubit. Two lowest levels $|0\rangle$ and $|1\rangle$ of the Xmon are applied as the qubit states. The frequency difference of qubit levels is $\omega_{10}/(2\pi) = 5.266\text{GHz}$. The relaxation time is $T_1 = 19.0\mu\text{s}$ and the pure dephasing time is $T_2^* = 10.0\mu\text{s}$. The readout fidelity of the ground state $|0\rangle$ and excited state $|1\rangle$ are $F_q^0 = 98.0\%$ and $F_q^1 = 93.6\%$, respectively.

Our protocol allows to experimentally realize an arbitrary nonadiabatic geometric one-qubit gate by a single loop. Our experiment specifically implements some certain nonadiabatic geometric gates, including identity operator I , Hadamard gate H , and rotation gates $R_x(\pi)$, $R_x(\pi/2)$, $R_y(\pi)$, $R_y(\pi/2)$, $R_z(\pi)$, as well as $R_z(\pi/2)$ with rotation axes denoted by x, y, z , and rotation angle denoted by $\pi, \pi/2$. In the process of realization, we input a resonant microwave pulse to manipulate the qubit. The rotation axis of geometric gates is adjusted by tuning microwave amplitude parameter $\Omega_R(t)$, microwave phase parameter φ , and evolution time τ_1 , τ_2 and τ . The rotation angle is adjusted by tuning microwave phase parameter γ . For each interval, $\Omega_R(t)$ is designed as $\Omega_R(t) = \Omega_0 \sin^2(\pi t/T)$ with the evolution period being taken as $T = 10\text{ns}$. With this specific design of $\Omega_R(t)$, the microwave pulse can be smoothly turned on and off at $\Omega_R(0)$ and $\Omega_R(T)$.

To characterize the performance of these nonadiabatic geometric gates, we apply quantum process tomography. In the quantum process tomography, we first prepare a set of initial states $\{|0\rangle, |1\rangle, (|0\rangle - i|1\rangle)/2, (|0\rangle + |1\rangle)/2\}$, by applying a set of operators $\{I, R_x(\pi), R_x(\pi/2), R_y(\pi/2)\}$ to the initialized state $|0\rangle$. These states are then followed by a specific nonadiabatic geometric gate. Finally, we perform measurement on the output states with standard quantum state tomography

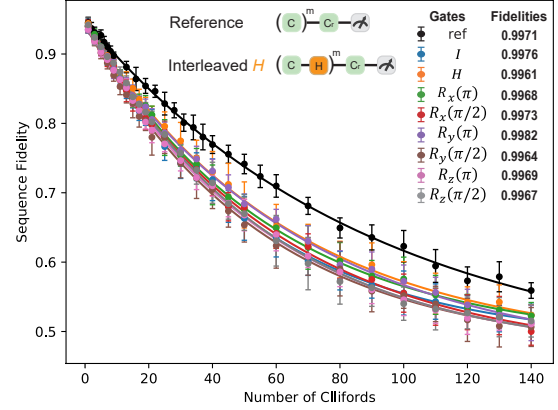


FIG. 3. (Color online) Clifford-based randomized benchmarking of nonadiabatic geometric gates.

and then reconstruct the output states. The whole process is shown in Fig. 2(a). In this process, a set of fixed basis operators $E_m \in \{I, \sigma_x, \sigma_y, \sigma_z\}$ is chosen to describe the quantum dynamical map $\varepsilon(\rho_i) = \sum_{mn} E_m \rho_i E_n \chi_{mn}$, where χ_{mn} is the process matrix that completely characterizes the behavior of quantum dynamics. By using the chosen initial states ρ_i and the reconstructed output states $\varepsilon(\rho_i)$, we can calculate the process matrix χ_{mn} . Compared this process matrix χ_{mn} with the ideal process matrix χ_{id} , we can obtain the process fidelity $F_p = \text{Tr}(\chi_{mn} \chi_{id})$. The matrix elements generated by the Hadamard gate H is shown in Fig. 2(b), and the process fidelity F_p of the realized nonadiabatic geometric gates is shown in Fig. 2(c). Accordingly, we can obtain the average process fidelity $\bar{F}_p = 99.6\%$. Please note that the measurement fidelity has been corrected in this fidelity to exclude the error from qubit state readout.

Clifford-based randomized benchmarking is different measurement, from which the gate fidelity can be separately extracted [60–62]. Specifically, we perform reference randomized benchmarking and interleaved randomized benchmarking. The former gives an average fidelity of the Clifford gates and the latter gives the fidelity of a specific gate.

First, we perform the reference randomized benchmarking, the process of which is shown in Fig. 3. Specifically, we initially prepare quantum states in ground state $|0\rangle$, which is then driven by randomly chosen m Clifford gates. Subsequently, a recovery gate is applied to reverse the operation of the m Clifford gates. Afterwards, we measure the state $|0\rangle$ and obtain its survival probability. Repeating this process by 50 times, we can achieve the average survival probability of state $|0\rangle$ as the function of m , which is known as sequence fidelity. The sequence fidelity F can be fitted by using the function $F = Ap^m + B$, where p is the depolarizing parameter, and A and B absorb the state preparation and measurement errors [61, 62]. Accordingly, we can achieve the depolarizing parameter p . The average error rate is then given by $r = (1 - p)/2$. From the result of the reference randomized benchmarking experiment, shown in Fig. 3, we obtain

$p = 0.994$, which yields average error rate $r = 0.003$ and the average fidelity of nonadiabatic geometric Clifford gates $\bar{F} = 99.7\%$.

Second, we perform the interleaved randomized benchmarking, the process of which is shown in Fig. 3. Specifically, we initially prepare quantum states in state $|0\rangle$. We then use m combination of a randomly chosen nonadiabatic geometric Clifford gate and a target nonadiabatic geometric gate to drive this state. Subsequently, a recovery gate is applied to reverse the above combination operation. Afterwards, we measure the state $|0\rangle$ and obtain its survival probability. With the similar procedure, we obtain a new depolarizing parameter p_g . The fidelity of a specific gate can be then calculated by using the function $F_g = 1 - (1 - p_g/p)/2$, where p is the depolarizing parameter obtained in the reference randomized benchmarking. Figure 3 shows the fidelities of the realized nonadiabatic geometric gates.

Up to now, we have completed the quantum process tomography and the Clifford-based randomized benchmarking for a set of nonadiabatic gates, the average fidelity of which is 99.7%.

IV. CONCLUSION

In conclusion, we have experimentally realized nonadiabatic geometric one-qubit gates I , H , $R_x(\pi)$, $R_x(\pi/2)$, $R_y(\pi)$,

$R_y(\pi/2)$, $R_z(\pi)$, and $R_z(\pi/2)$ with superconducting Xmon qubits. The average fidelities of these gates can be up to 99.6% and 99.7% characterized by quantum process tomography and randomized benchmarking, respectively. Different from nonadiabatic holonomic gates realized with three-level quantum systems, our experiment is performed on two lowest levels of an Xmon qubit and thus avoids the influence from the short coherence time of the second excited state. The methods and techniques used here can be extended to the other quantum systems, such as nuclear magnetic resonance, trapped ions, and nitrogen-vacancy centers in diamond.

ACKNOWLEDGMENTS

The work reported here was supported by the National Basic Research Program of China (Grants No. 2015CB921004), the National Key Research and Development Program of China (Grant No. 2016YFA0301700), the National Natural Science Foundation of China (Grants No. 11775129, No. 11575101, and No. 11934010), and the Anhui Initiative in Quantum Information Technologies (Grant No. AHY080000). This work was partially conducted at the University of Science and Technology of the China Center for Micro- and Nanoscale Research and Fabrication.

-
- [1] M. J. Bremner, C. M. Dawson, J. L. Dodd, A. Gilchrist, A. W. Harrow, Phys. Rev. Lett. **89**, 247902 (2002).
 - [2] G. D. Chiara and G. M. Palma, Phys. Rev. Lett. **91**, 090404 (2003).
 - [3] A. Carollo, I. F. Guridi, M. F. Santos, and V. Vedral, Phys. Rev. Lett. **92**, 020402 (2004).
 - [4] P. Solinas, P. Zanardi, and N. Zanghi, Phys. Rev. A **70**, 042316 (2004).
 - [5] S. L. Zhu and P. Zanardi, Phys. Rev. A **72**, 020301(R) (2005).
 - [6] J. T. Thomas, M. Lababidi, and M. Tian, Phys. Rev. A **84**, 042335 (2011).
 - [7] M. Johansson, E. Sjöqvist, L. M. Andersson, M. Ericsson, B. Hessmo, K. Singh, and D. M. Tong, Phys. Rev. A **86**, 062322 (2012).
 - [8] P. Zanardi and M. Rasetti, Phys. Lett. A **264**, 94 (1999).
 - [9] J. A. Jones, V. Vedral, A. Ekert, and G. Castagnoli, Nature **403**, 869 (2000).
 - [10] L. M. Duan, J. I. Cirac, and P. Zoller, Science **292**, 1695 (2001).
 - [11] M. V. Berry, Proc. R. Soc. London Ser. A **392**, 45 (1984).
 - [12] F. Wilczek and A. Zee, Phys. Rev. Lett. **52**, 2111 (1984).
 - [13] X. B. Wang and M. Keiji, Phys. Rev. Lett. **87**, 097901 (2001).
 - [14] S. L. Zhu and Z. D. Wang, Phys. Rev. Lett. **89**, 097902 (2002).
 - [15] Y. Aharonov and J. Anandan, Phys. Rev. Lett. **58**, 1593. (1987).
 - [16] E. Sjöqvist, D. M. Tong, L. M. Andersson, B. Hessmo, M. Johansson, and K. Singh, New J. Phys. **14**, 103035 (2012).
 - [17] G. F. Xu, J. Zhang, D. M. Tong, E. Sjöqvist, and L. C. Kwek, Phys. Rev. Lett. **109**, 170501 (2012).
 - [18] J. Anandan, Phys. Lett. A **133**, 171 (1988).
 - [19] S. L. Zhu and Z. D. Wang, Phys. Rev. Lett. **91**, 187902 (2003).
 - [20] X. L. Feng, C. F. Wu, H. Sun, and C. H. Oh, Phys. Rev. Lett. **103**, 200501 (2009).
 - [21] Y. Ota and Y. Kondo, Phys. Rev. A **80**, 024302 (2009).
 - [22] J. Spiegelberg and E. Sjöqvist, Phys. Rev. A **88**, 054301 (2013).
 - [23] G. F. Xu and G. L. Long, Phys. Rev. A **90**, 022323 (2014).
 - [24] Z. T. Liang, Y. X. Du, W. Huang, Z. Y. Xue, and H. Yan, Phys. Rev. A **89**, 062312 (2014).
 - [25] Z. Y. Xue, J. Zhou, and Z. D. Wang, Phys. Rev. A **92**, 022320 (2015).
 - [26] G. F. Xu, C. L. Liu, P. Z. Zhao, and D. M. Tong, Phys. Rev. A **92**, 052302 (2015).
 - [27] E. Sjöqvist, Phys. Lett. A **380**, 65 (2016).
 - [28] V. V. Albert, C. Shu, S. Krastanov, C. Shen, R. B. Liu, Z. B. Yang, R. J. Schoelkopf, M. Mirrahimi, M. H. Devoret, and L. Jiang, Phys. Rev. Lett. **116**, 140502 (2016).
 - [29] P. Z. Zhao, G. F. Xu, and D. M. Tong, Phys. Rev. A **94**, 062327 (2016).
 - [30] E. Herterich and E. Sjöqvist, Phys. Rev. A **94**, 052310 (2016).
 - [31] P. Z. Zhao, G. F. Xu, Q. M. Ding, E. Sjöqvist, and D. M. Tong, Phys. Rev. A **95**, 062310 (2017).
 - [32] P. Z. Zhao, X. D. Cui, G. F. Xu, E. Sjöqvist, and D. M. Tong, Phys. Rev. A **96**, 052316 (2017).
 - [33] P. Z. Zhao, X. Wu, T. H. Xing, G. F. Xu, and D. M. Tong, Phys. Rev. A **98**, 032313 (2018).
 - [34] P. Z. Zhao, G. F. Xu, and D. M. Tong, Phys. Rev. A **99**, 052309 (2019).
 - [35] D. Leibfried, B. DeMarco, V. Meyer, D. Lucas, M. Barrett, J. Britton, W. M. Itano, B. Jelenkovic, C. Langer, T. Rosenband, and D. J. Wineland, Nature **422**, 412 (2003).

- [36] J. F. Du, P. Zou, and Z. D. Wang, *Phys. Rev. A* **74**, 020302 (2006).
- [37] G. R. Feng, G. F. Xu, and G. L. Long, *Phys. Rev. Lett.* **110**, 190501 (2013).
- [38] H. Li, Y. Liu, and G. L. Long, *Sci. China-Phys. Mech. Astron.* **60**, 080311 (2017).
- [39] A. A. Abdumalikov, J. M. Fink, K. Juliusson, M. Pechal, S. Berger, A. Wallraff, and S. Filipp, *Nature* **496**, 482 (2013).
- [40] Y. Xu, W. Cai, Y. Ma, X. Mu, L. Hu, T. Chen, H. Wang, Y. P. Song, Z. Y. Xue, Z. Q. Yin, and L. Sun, *Phys. Rev. Lett.* **121**, 110501 (2018).
- [41] Z. X. Zhang, P. Z. Zhao, T. H. Wang, L. Xiang, Z. L. Jia, P. Duan, D. M. Tong, Y. Yin and G. P. Guo, *New J. Phys.* **21**, 073024 (2019)
- [42] S. Danilin, A. Vepsäläinen, and G. S. Paraoanu, *Phys. Scr.* **93**, 055101 (2018).
- [43] D. J. Egger, M. Ganzhorn, G. Salis, A. Fuhrer, P. Müller, P. Kl. Barkoutsos, N. Moll, I. Tavernelli, and S. Filipp, *Phys. Rev. Appl.* **11**, 014017 (2019).
- [44] C. Zu, W. B. Wang, L. He, W. G. Zhang, C. Y. Dai, F. Wang, and L. M. Duan, *Nature* **514**, 72 (2014).
- [45] S. A. Camejo, A. Lazariiev, S. W. Hell, and G. Balasubramanian, *Nat. Commun.* **5**, 4870 (2014).
- [46] B. B. Zhou, Paul C. Jerger, V. O. Shkolnikov, F. J. Heremans, Guido Burkard, and David D. Awschalom, *Phys. Rev. Lett.* **119**, 140503 (2017).
- [47] Y. Sekiguchi, N. Niikura, R. Kuroiwa, H. Kano, and H. Kosaka, *Nat. Photonics* **11**, 309 (2017).
- [48] K. Nagata, K. Kuramitani, Y. Sekiguchi, and H. Kosaka, *Nat. Commun.* **9**, 3227 (2018).
- [49] N. Ishida, T. Nakamura, T. Tanaka, S. Mishima, H. Kano, R. Kuroiwa, Y. Sekiguchi, and H. Kosaka, *Opt. Lett.* **43**, 2380 (2018).
- [50] J. Zhang, T. H. Kyaw, D. M. Tong, E. Sjöqvist, and L. C. Kwek, *Sci. Rep.* **5**, 18414 (2015).
- [51] Z. T. Liang, X. X. Yue, Q. X. Lv, Y. X. Du, W. Huang, H. Yan, and S. L. Zhu, *Phys. Rev. A* **93**, 040305(R) (2016).
- [52] M. V. Berry, *J. Phys. A: Math. Theor.* **42**, 365303 (2009).
- [53] F. Kleiβler, A. Lazariiev, and S. A. Camejo, *npj Quantum Inf.* **4**, 49 (2018).
- [54] T. X. Yan, B. J. Liu, K. Xu, C. Song, S. Liu, Z. S. Zhang, H. Deng, Z. G. Yan, H. Rong, K. Q. Huang, M. H. Yung, Y. Z. Chen, and D. P. Yu, *Phys. Rev. Lett.* **122**, 080501 (2018).
- [55] T. H. Wang, Z. X. Zhang, L. Xiang, Z. L. Jia, P. Duan, W. Z. Cai, Z. H. Gong, Z. W. Zong, M. M. Wu, J. L. Wu, L. Y. Sun, Y. Yin and G. P. Guo, *New J. Phys.* **20**, 065003 (2018)
- [56] J. Koch, T. M. Yu, J. Gambetta, A. A. Houck, D. I. Schuster, J. Majer, Alexandre Blais, M. H. Devoret, S. M. Girvin, and R. J. Schoelkopf, *Phys. Rev. A* **76**, 042319 (2007).
- [57] R. Barends, J. Kelly, A. Megrant, D. Sank, E. Jeffrey, Y. Chen, Y. Yin, B. Chiaro, J. Mutus, C. Neill, P. O'Malley, P. Roushan, J. Wenner, T. C. White, A. N. Cleland, and J. M. Martinis, *Phys. Rev. Lett.* **111**, 080502 (2013).
- [58] R. Barends, J. Kelly, A. Megrant, A. Veitia, D. Sank, E. Jeffrey, T. C. White, J. Mutus, A. G. Fowler, B. Campbell, Y. Chen, Z. Chen, B. Chiaro, A. Dunsworth, C. Neill, P. O'Malley, P. Roushan, A. Vainsencher, J. Wenner, A. N. Korotkov, A. N. Cleland, and J. M. Martinis, *Nature* **508**, 500 (2014).
- [59] J. Kelly, R. Barends, A. G. Fowler, A. Megrant, E. Jeffrey, T. C. White, D. Sank, J. Y. Mutus, B. Campbell, Y. Chen, Z. Chen, B. Chiaro, A. Dunsworth, I. C. Hoi, C. Neill, P. J. J. O'Malley, C. Quintana, P. Roushan, A. Vainsencher, J. Wenner, A. N. Cleland, and J. M. Martinis, *Nature* **519**, 66 (2015).
- [60] J. M. Chow, J. M. Gambetta, L. Tornberg, J. Koch, L. S. Bishop, A. A. Houck, B. R. Johnson, L. Frunzio, S. M. Girvin, and R. J. Schoelkopf, *Phys. Rev. Lett.* **102**, 090502 (2009).
- [61] E. Magesan, J. M. Gambetta, and J. Emerson, *Phys. Rev. Lett.* **106**, 180504 (2011).
- [62] E. Magesan, J. M. Gambetta, B. R. Johnson, C. A. Ryan, J. M. Chow, S. T. Merkel, M. P. da Silva, G. A. Keefe, M. B. Rothwell, T. A. Ohki, M. B. Ketchen, and M. Steffen, *Phys. Rev. Lett.* **109**, 080505 (2012).